Research article

Immunomodulatory biomimetic nanoparticles target articular cartilage trauma after systemic administration

Chiara Mancino [a,b,c], Anna Pasto [d], Enrica De Rosa [a,b], Luigi Dolcetti [d], Marco Rasponi [c], Patrick McCulloch [b], Francesca Taraballi [a,b,*]

[a] Center for Musculoskeletal Regeneration, Houston Methodist Academic Institute, Houston, TX, USA
[b] Orthopedics and Sports Medicine, Houston Methodist Hospital, Houston, TX, USA
[c] Department of Electronics, Information and Bioengineering, Politecnico di Milano, Milano, Italy
[d] Richard Dimbleby Laboratory of Cancer Research, School of Cancer & Pharmaceutical Sciences, King's College London, London, UK

A B S T R A C T

Post-traumatic osteoarthritis (PTOA) is one of the leading causes of disability in developed countries and accounts for 12% of all osteoarthritis cases in the United States. After trauma, inflammatory cells (macrophages amongst others) are quickly recruited within the inflamed synovium and infiltrate the joint space, initiating dysregulation of cartilage tissue homeostasis. Current therapeutic strategies are ineffective, and PTOA remains an open clinical challenge. Here, the targeting potential of liposome-based nanoparticles (NPs) is evaluated in a PTOA mouse model, during the acute phase of inflammation, in both sexes. NPs are composed of biomimetic phospholipids or functionalized with macrophage membrane proteins. Intravenous administration of NPs in the acute phase of PTOA and advanced *in vivo* imaging techniques reveal preferential accumulation of NPs within the injured joint for up to 7 days post injury, in comparison to controls. Finally, imaging mass cytometry uncovers an extraordinary immunomodulatory effect of NPs that are capable of decreasing the amount of immune cells infiltrating the joint and conditioning their phenotype. Thus, biomimetic NPs could be a powerful theranostic tool for PTOA as their accumulation in injury sites allows their identification and they have an intrinsic immunomodulatory effect.

1. Introduction

Osteoarthritis (OA) is one of the most prevalent chronic diseases in developed countries and, in the United States alone, around 27 million adults over 25 years old have been diagnosed with OA of any joint [1–3]. In approximately 12% of OA cases, symptoms arise after joint injury: when OA develops after a trauma, it is defined as post-traumatic OA (PTOA). Direct costs for PTOA treatments reached peaks of $3 billions annually and, as joint injury rates increase, so will the financial burden on the healthcare system.

Damage from injury triggers a local inflammatory response that results in cartilage degeneration and progressive joint instability [3–5]. The acute and subacute phases of inflammation can last for up to 1.5 months post injury and are characterized by increased expression of pro-inflammatory cytokines and proteolytic enzymes, which contribute to catabolic effects on resident cells and extracellular matrix degradation [3,5,6]. When the acute phase of inflammation is not resolved, a chronic state of inflammation occurs

---

i) Leukocytes (J774)
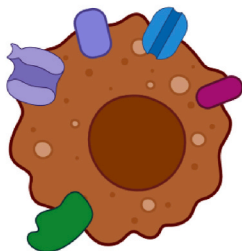
ii) Membrane protein (MP) extraction
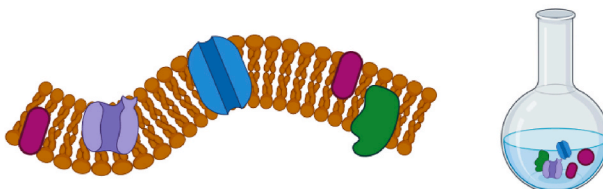
iii) Dried lipid film formation:
- DPPC
- CHOLESTEROL
- DSPC
- DOPG
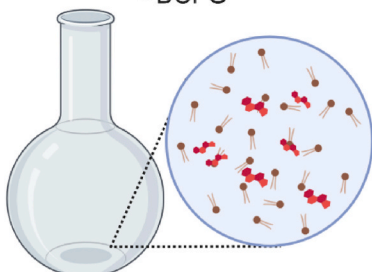
iv) Hydration with MPs

v) Orthosome formation after extrusion

IVIS: Quantification of fluorescence signal form NPs accumulation in legs and filter organs

IVM: Qualitative evaluation of NPs accumulation in the joint space

IMC: Quantitative evaluation of inflammatory markers withy Hyperion system

vi) PTOA mouse model: Surgical Disruption of Medial Meniscus (DMM)

C75BL/6 mice male & female

vii) IV administration of Orthosomes/Liposomes (retro-orbital)

NPs fluorescently labeled adminstered 24h, 48, 72h, 7days after trauma

(caption on next page)

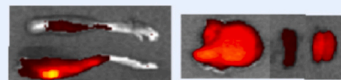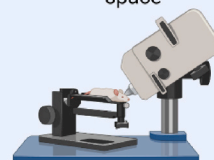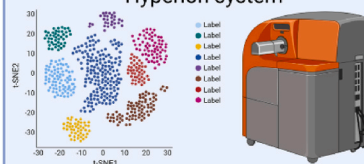**Fig. 1.** Schematic of NP synthesis and experimental setup for *in vivo* experiments. LIPO and ORTHO were synthesized *via* Thin Layer Evaporation. J774 leukocytes (i) were used to extract MPs (ii). A dried lipid film with the selected phospholipids was obtained (iii) and hydrated with an aqueous phase containing 1× PBS (LIPO) or 1× PBS with J774 macrophage MPs (ORTHO) (iv). Formulations were extruded through polycarbonate membranes of decreasing pore size to achieve good control of physiochemical properties (v). We hypothesized that systemic administration of ORTHO would lead to accumulation of NPs in the injured joint, and we tested this hypothesis by administering ORTHO IV to a surgically induced PTOA murine model (vi, vii) between 24 h and 7 d post injury and evaluating their targeting and biodistribution with IVIS, the NPs extravasation within the injured joint with IVM, and the immunomodulatory effect via IMC.

in which many inflammatory players (neutrophils, macrophages, synoviocytes) trigger a perpetual cycle of local tissue damage, inflammation, and repair, similar to the one that occurs in chronic wounds [3,5,7]. The combination of these early events can ultimately result in loss of function, alongside joint stiffness, pain, and disability [8]. Current therapies remain ineffective, mostly providing some palliative care or pain management. A treatment capable of slowing down or reversing the progression of the disease is yet to be found, leaving patients with surgical interventions (arthroplasties, osteotomies, joint fusions, and joint replacements) as their only option [5]. Recent studies have investigated the use of nanomedicine to develop drug delivery systems for OA. Nanomedicine can offer extraordinary advantages [9–11]: nanoscale carriers can effectively deliver a variety of drugs to specific locations, allowing (i) selective targeting of disease sites, (ii) decreased off-target toxicity, (iii) increased drug stability and circulation time within the body (they can be tailored to achieve immune system escape), and (iv) improved cell internalization of the cargo. Notably, lipid-based nanocarriers known as liposomes have shown improved pharmacological and pharmacokinetic efficiency compared with drugs alone, in treating a variety of conditions such as acute myeloid leukemia, pain management, ovary, gastric, breast, lung cancer, and OA [12]. In fact, nanoparticles (NPs) can be used to encapsulate disease-modifying drugs and biomolecules capable of addressing chondrocyte activity and/or synovial inflammation. In this scenario, one of the biggest challenges in drug delivery for OA is the selective targeting of the affected joint/s: the easiest way to overcome it is intra-articular administration [13]. Although somewhat effective, intra-articular administration has some limitations related to low retention of the administered agents that are prone to easily escape the joint and be drained by the lymphatic system [14,15]. This requires repeated intra-articular injections, which can be painful for patients. In addition, PTOA patients likely have multiple sites of trauma, also requiring repeated injections in multiple sites, which can become a burden. In this scenario, systemic administration of NPs capable of targeting multiple sites of trauma would be ideal.
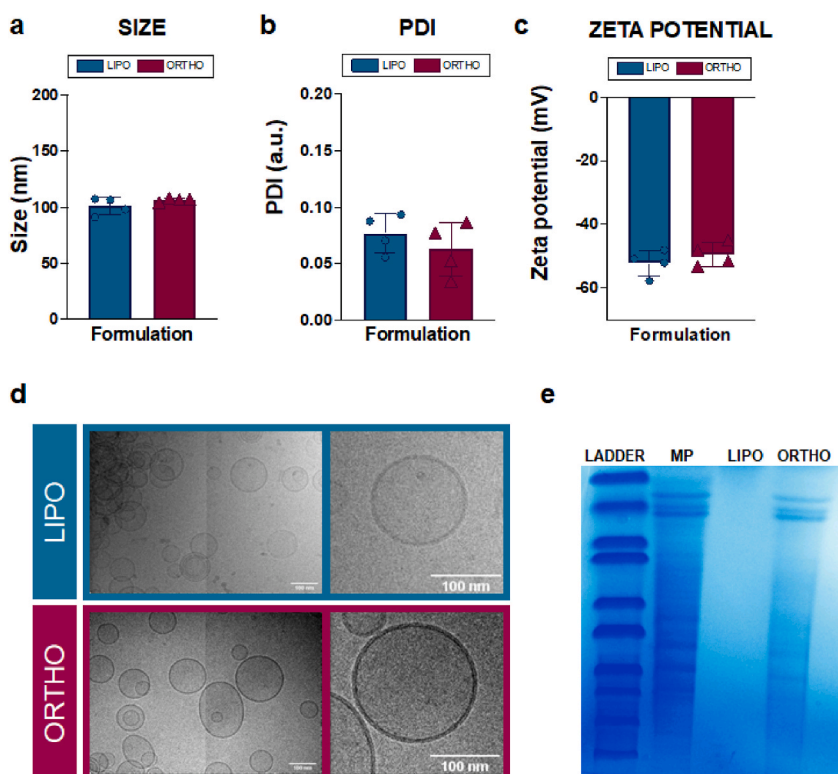
Fig. 2. Characterization of the physiochemical properties of NPs. After synthesis, Dynamic Light Scattering was used to assess the physiochemical properties of LIPO and ORTHO. (a) Size of NPs (~100 nm), (b) PDI, and (c) zeta potential were unaffected by the incorporation of MPs in the formulation. (d) Cryo-TEM assessment confirmed that there was no morphological change following the incorporation of MPs (scalebars 100 nm). (e) SDS-Page showed that the protein profile of MPs was maintained by ORTHO, proving successful incorporation of MPs. Data was analyzed with unpaired t-student test (p ≤ 0.05 was the threshold for statistical significance) and is shown as mean ± SD.

Recently, biomimetic NPs have been explored to address the targeting challenge [16,17]. Liposome-based NPs are intrinsically biomimetic when synthesized with phospholipids that can be found within natural cell membranes, such as phosphatidylcholine (PC), phosphatidylethanolamine (PE), phosphatidylglycerol (PG), and phosphatidylserine (PS) [18]. The addition of membrane proteins (MPs) gives these NPs an extra layer of biomimicry [19]. We recently explored the use of leukocyte MPs to increase targeting towards inflammation [16,20–25]. These NPs give us unique leverage on the targeting of inflammation sites: macrophages are one of the first cell types recruited to an inflammation site, and we showed that this behavior was retained by our biomimetic NPs [26,27].

In the present work, we assessed the targeting potential of NPs in a PTOA mouse model, during the acute phase of the inflammation. For the purpose of this study, NPs functionalized with MPs were called orthosomes (ORTHO), while biomimetic liposomes (LIPO) were used as a control (Fig. 1i–v). As mentioned above, the acute phase of inflammation following joint trauma is characterized by increased expression of pro-inflammatory cytokines and increased vascularization within the injury site/s. We hypothesized that systemic administration of ORTHO would lead to accumulation of NPs in the injured joint. We tested this hypothesis in a surgically induced PTOA murine model by administering ORTHO intravenously (IV) between 24 h and 7 days post injury and evaluating their targeting and biodistribution (Fig. 1vi–vii). Additionally, given the sex-dependent severity of PTOA in humans, where females display higher prevalence and severity of symptoms [28], we compared NP accumulation in both sexes.
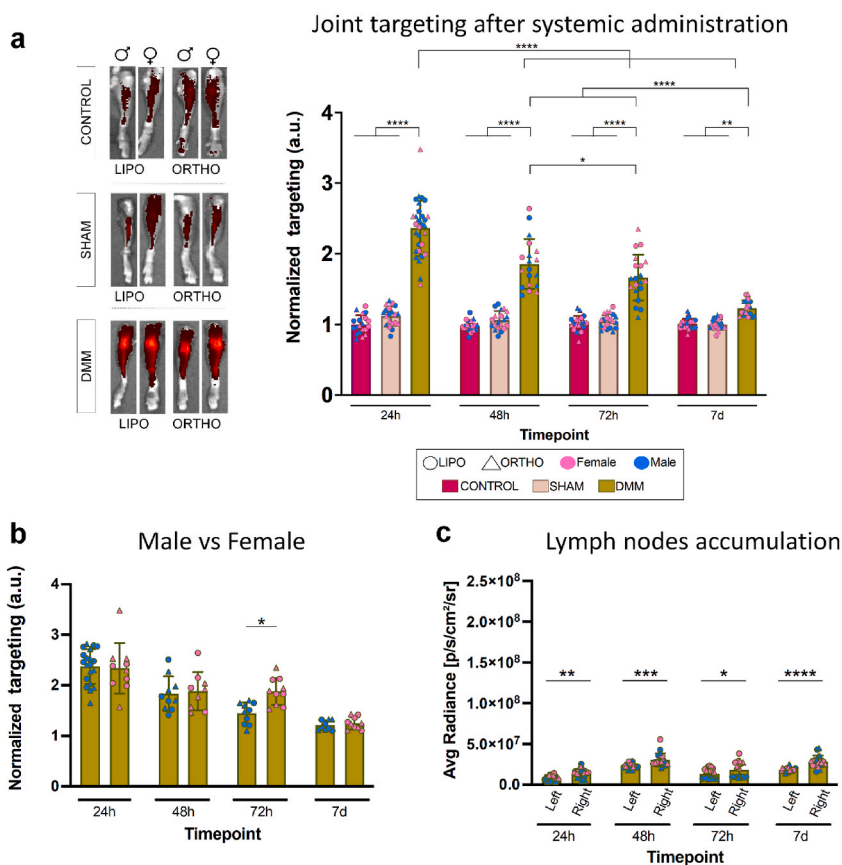
Fig. 3. *Ex vivo* targeting of the injured leg using IVIS (a) Normalized targeting signals of NPs towards the injured leg 6 h after systemic administration. Mice were injected retro-orbitally at 24 h, 48 h, 72 h, and 7 d post DMM on their right leg, then sacrificed 6 h post injection. Left and right legs were imaged *ex vivo* using IVIS. Signal from the right leg was divided by the one from the left leg (internal healthy control) to obtain the normalized targeting signal (see picture panel that shows a typical outcome of the image acquisition using IVIS). There was a significantly higher accumulation of NPs (LIPO and ORTHO) in the injured leg for up to 7 d post injury (p < 0.0001 for the 24–72 h timepoints, and p < 0.003 for the 7 d timepoint) compared with the CONTROL and SHAM groups. (b) Evaluation of sex-related differences in normalized targeting signal for the DMM group. Accumulation of NPs within the injured leg was significantly higher in the female mice only at the 72 h post-injury timepoint (p < 0.05). (c) Accumulation of NPs within inguinal lymph nodes for the DMM group. NP accumulation was significantly higher in the right lymph node, the same side of the injured leg (p < 0.04 or less. Data were analyzed with two-way ANOVA followed by Tukey's multiple comparisons test (p ≤ 0.05 was the threshold for statistical significance) and are shown as mean ± SD (a: n = 20, except for the DMM group at 24 h, where n = 30; b: n = 10, except for the male DMM group at 24 h, where n = 20; c: n = 20, except for the DMM group at 24 h, where n = 30).

2. Results and discussion

2.1. NP synthesis and characterization

LIPO and ORTHO were synthesized via Thin Layer Evaporation (Fig. 1) to achieve good control over the NPs' physiochemical properties as well as reproducibility. While LIPO are intrinsically biomimetic, their lipid composition being similar to the one present in the cell membrane, ORTHO incorporate macrophage MPs from the J774 monocyte cell line, giving ORTHO an extra layer of bio-mimicry by inserting a biological element within the corona of the NPs. Both NPs were characterized for size, polydispersity index (PDI), and surface charge (zeta potential). Size of NPs was ~100 nm (100.9 ± 7.7 nm and 106.7 ± 1.5 nm for LIPO and ORTHO, respectively, Fig. 2a), and protein incorporation during ORTHO fabrication, at a protein-lipid ratio of 1 : 40, did not have a significant effect on their size or PDI. After Thin Layer Evaporation, NPs were extruded to achieve PDIs as low as 0.08 ± 0.02 a.u. for LIPO and 0.06 ± 0.02 a.u. for ORTHO (Fig. 2b), making NPs particularly suitable for *in vivo* application, given the homogenous distribution. The zeta potential was consistently below −45 mV (−52.1 ± 4.1 mV and −49.5 ± 3.7 mV for LIPO and ORTHO, respectively, Fig. 2c), thus increasing electrical double layer repulsive forces between vesicles and making these NPs less prone to aggregation [29].

Cryo-Transmission Electron Microscopy (Cryo-TEM) images showed that both LIPO and ORTHO are homogeneous in size and mostly unilamellar (Fig. 2d). The incorporation of MPs did not have any effect on NP morphology and phospholipid bilayer thickness, consistent with reported formulations [21,26,27,30]. To visualize the localization of NPs after systemic injection with the In Vivo Imaging System (IVIS) and Intravital Microscopy (IVM), we incorporated a small amount of fluorescently labeled lipid (Cy7-conjugated and Cy5.5-conjugated, respectively), which did not affect NP shape or membrane integrity.

Finally, evidence of MP incorporation within the ORTHO corona was gathered via Coomassie blue: while no protein band was identified in LIPO, ORTHO maintained the same protein profile present in the MP stock (Fig. 2e).

2.2. In vivo NP targeting to the injured knee joint

To test the NPs' capability of targeting PTOA injury sites in the acute phase post trauma, we selected a translational and well-established surgically induced PTOA mouse model: the Disruption of Medial Meniscus (DMM) [31]. Medial meniscus bears more load during normal ambulation in mice and, when damaged, causes changes in load distribution within the joint, and joint instability arises. This, combined with other factors, such as the actual injury and subsequent inflammation, causes progression of the pathology, with full symptoms of PTOA appearing 4–6 weeks post injury. Immediately after injury, neovascularization is one of the first phenomena that arise in the synovium, while macrophages and other immune cells are steadily recruited to the inflamed synovium [32, 33].

DMM surgery was performed on both male and female mice, to account for possible sex differences. The right leg underwent DMM surgery, and the left leg was used as internal, healthy control. While NPs are a powerful tool to selectively target inflammation, it is important to evaluate whether any secondary factor, like a skin incision, could affect their preferential accumulation. Thus, we included a SHAM group, where the surgery simply involved a skin incision, and a CONTROL group, where mice were left undisturbed prior to IV administration of NPs. We IV administered Cy7-labeled NPs, accessing the blood stream via retro-orbital sinus, at 24 h, 48 h, 72 h, and 7 d post injury. Since NP accumulation in the inflammation site peaks between 6 and 8 h post IV injection [26,27], animals were sacrificed 6 h post injection, and their organs and legs were imaged *ex vivo* using IVIS (Supplementary Fig. S1). Results revealed preferential accumulation of both LIPO and ORTHO within the injured leg. Normalized fluorescence signal, obtained by dividing the signal from the injured right leg by the one from the internal control (left leg), was significantly higher for up to 7 d post injury relative to the CONTROL and SHAM groups (p < 0.0001 for the 24–72 h timepoints and p < 0.003 for the 7 d timepoint, Fig. 3a). Normalizing the fluorescence signal of the injured leg by the internal control enabled us to assess only the relative accumulation of the signal, removing variables such as mouse weight and intra-litter variability. We hypothesize that increased vascularization after an injury is the primary mechanism of NP accumulation in the injured leg. This is supported by the fact that the signal decreased over time, while the injury was healing. Surprisingly, there was no significant difference in targeting between LIPO and ORTHO (Supplementary Fig S2): IVIS resolution might not be able to discriminate these differences from signals emitted from the whole organ. There were also no significant differences in NP accumulation between male and female mice (Fig. 3b and Supplementary Fig. S2b), despite evidence of worse symptoms of PTOA in female patients [34]. This highlights how using animal models to study human pathologies can have intrinsic limitations, especially for orthopedic applications, because there is often lack of correlation between the animal model and human pathology [35]. Moreover, information on sex-dependent differences in OA development for the DMM model is limited. Nevertheless, DMM is still one of the most accepted small-animal models of PTOA to date, particularly because it ensures slow pathology progression, and it is capable of mimicking OA development due to joint instability after injury [2]. Remarkably, inguinal lymph nodes showed a trend of increased NP accumulation only on the side corresponding to the injury (right lymph node) with the NP signal being significantly higher for up to 7 d post injury (p < 0.04, Fig. 3c).

Taken together, these findings validate our hypothesis on the use of biomimetic NPs for systemic targeting of injuries in the acute phase of PTOA. Despite the absence of a significant difference in NP accumulation between LIPO and ORTHO, there might be some effect of immunomodulation at a later timepoint due to the ability of ORTHO to mimic leukocytes, as these NPs trigger immunomodulation in a different traumatic murine model [36].

## 2.3. NP biodistribution after systemic injection

It is important to evaluate the biodistribution of a systemically administered substance to identify any non-specific accumulation in off-target areas, which could trigger unwanted side effects in areas with high accumulation. Here, we evaluated the NPs' biodistribution in the CONTROL, SHAM, and DMM groups *ex vivo*, 6 h post administration. Peripheral organs (heart, lungs, liver, spleen, kidneys, and lymph nodes) were collected 6 h post injection and imaged using IVIS (Supplementary Figure S1). Our results show preferential accumulation of both LIPO and ORTHO in filtering organs, consistently with the extensive literature showing NPs with sizes <200 nm preferentially accumulating in those organs when injected systemically [37]. The highest signal was in the liver, followed by kidneys, spleen, and lungs, and there was no significant difference between timepoints (Fig. 4a–d and Supplementary Fig. S4). Histological sections of filtering organs (liver, spleen, and kidneys) stained with hematoxylin and eosin (H&E; Supplementary Fig. S5) showed no damage and no sign of toxicity following systemic administration. It has been suggested that specific pathologies not only influence the main organ of interest but also peripheral organs [36]. This interesting phenomenon was not observed in DMM.

2.4. NP extravasation in the injured knee joint

Insight on the accumulation of NPs within the injured leg was obtained by IVM which is comprised of a built-in anesthesia system that allowed us to follow NP signal accumulation in the injured leg for up to 6 h post injection. To the best of our knowledge, this was the first attempt at *in vivo* live microscopy of a mouse knee joint, and this strategy has great potential for supporting and improving the field of biomaterials for cartilage regeneration. For the purpose of this experiment, anesthetized mice were placed in a supine position, and the synovial capsule was exposed in both the injured leg and the left leg (internal control, Fig. 5a). We were able to identify the suture material added during surgery to ensure proper image acquisitions from the area of interest (Fig. 5b). Despite the presence of some aspecific extravasation of NPs in the left leg, it is possible to qualitatively appreciate a higher degree of accumulation, and
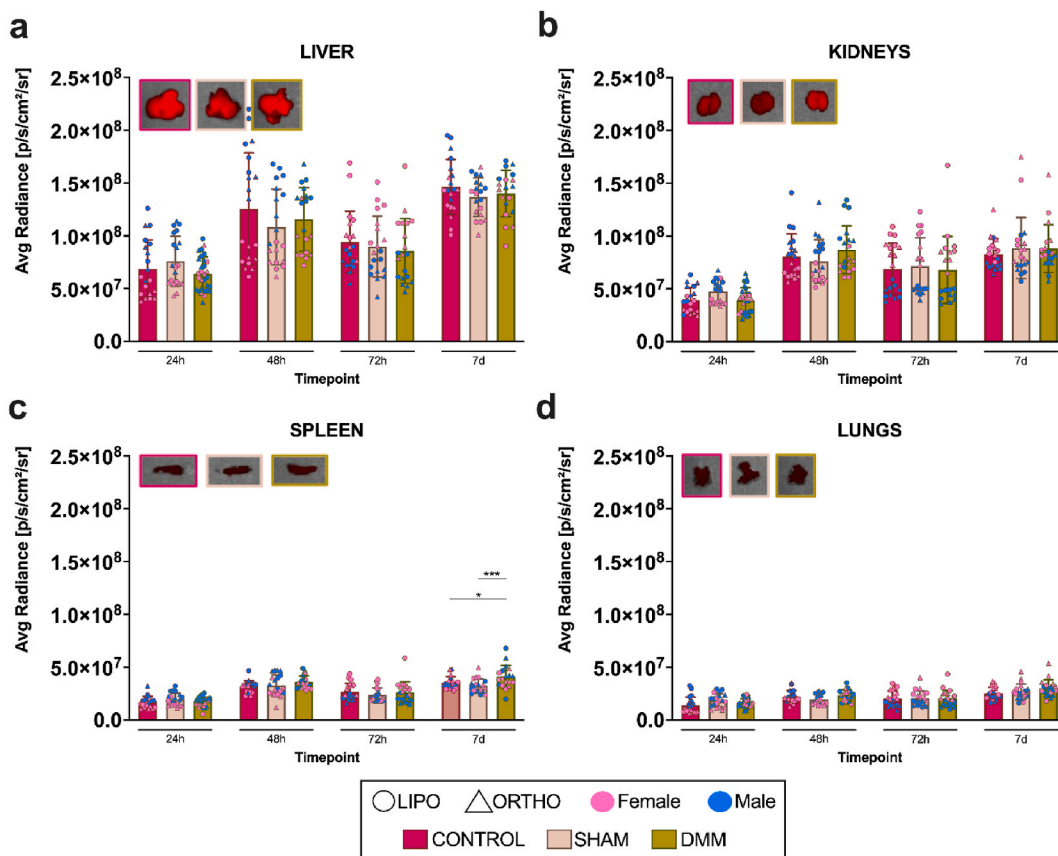
Fig. 4. *Ex vivo* biodistribution after injury. *Ex vivo* NP accumulation in the major filtering organs, the (a) liver, (b) kidneys, and (c) spleen, and in the (d) lungs 6 h post systemic administration, with corresponding representative IVIS images. Mice were IV administered LIPO and ORTHO at 24 h, 48 h, 72 h, and 7 d post surgery and sacrificed 6 h post injection. There was no significant difference in peripheral organ accumulation of NPs between the DMM group and the SHAM or CONTROL groups except for the spleen 7 d post injury where NP accumulation in the DMM was significantly higher ($p < 0.05$ or lower). Data were analyzed with two-way ANOVA followed by Tukey's multiple comparisons test ($p \leq 0.05$ was the threshold for statistical significance) and are shown as mean ± SD (n = 20, except for the DMM group at 24 h, where n = 30).
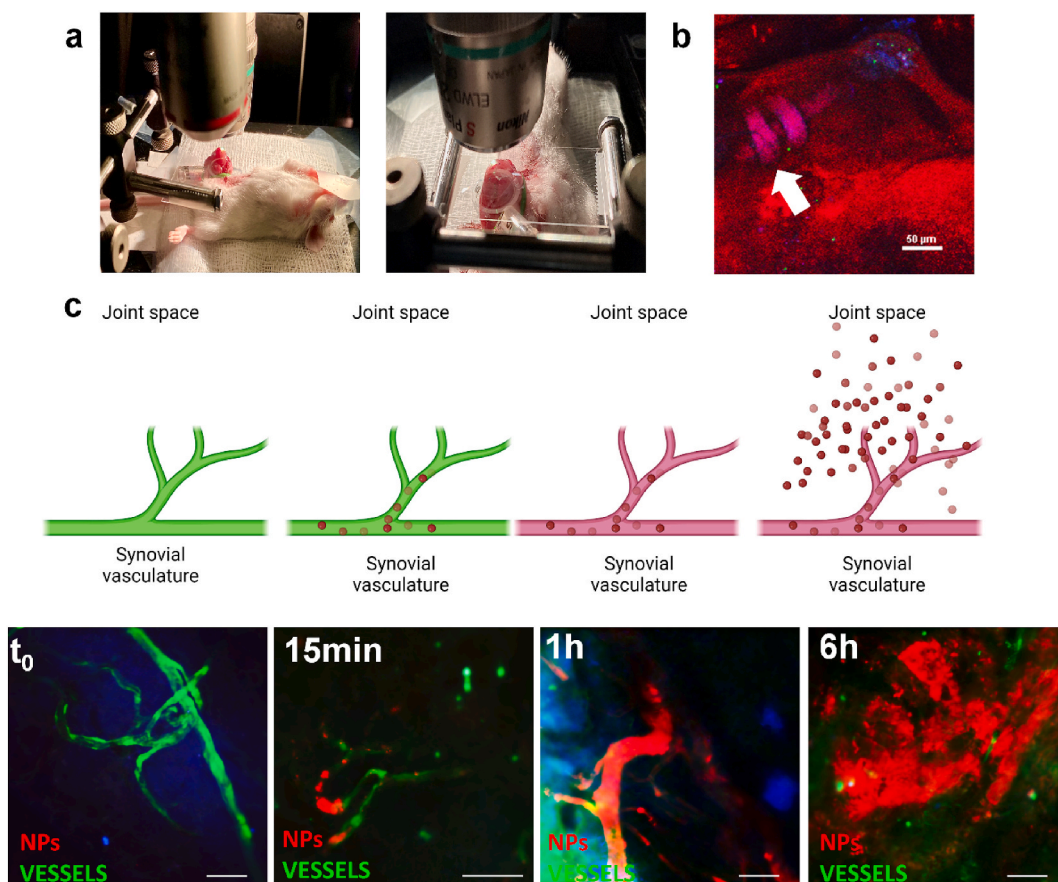
Fig. 5. NP extravasation in the injured knee joint using IVM. To assess the NPs' ability to target the inflamed synovium, we imaged mice with IVM at the time of injection (t_0) as well as 15min, 1 h, and 6 h post administration. (a) Anesthetized mice were placed in a supine position, and the synovial capsule was exposed for the injured leg and the left leg (internal control). (b) The suture is clearly visible within the imaged region. (c) It is possible to qualitatively appreciate a higher degree of accumulation, and therefore extravasation, of NPs (in red) within the injured leg, as shown in the schematic and microscopy images (vessels appear in green). Scalebars 50 nm. (For interpretation of the references to color in this figure legend, the reader is referred to the Web version of this article.)

therefore extravasation, within the injured leg at 6 h post administration (Fig. 5c). This phenomenon could be an extremely powerful strategy for delivering therapeutics to injured joints. In fact, the synovial capsule is the main source of analyte exchange for avascular, aneural, and alymphatic cartilage, and increased permeability of the synovial vasculature has been shown to occur mainly after injury [38].

2.5. Histology

Histological sections of treated and untreated joints stained with H&E (Fig. 6) validated the presence of articular cartilage damage following injury. As indicated by the green arrows, only the DMM group showed some extent of cartilage damage, while the SHAM group's articular cartilage was untouched and healthy. Notably, DMM mice only develop OA symptoms 4–6 weeks post injury, while the goal of this study was the evaluation of the acute cartilage trauma occurring immediately after injury that could model meniscal tears in humans.

2.6. Immune response after trauma: imaging mass cytometry (IMC)

Development of PTOA has long been associated with a complex biological response that not only involves mechanical injury and biomechanics but also inflammation: the immune system itself, in fact, plays a big role in the pathophysiology of PTOA [39–41]. Cellular infiltrates from both the innate and adaptive immune systems are consistently recruited in the synovial space after trauma, and they initiate an inflammatory cascade that triggers upregulation of catabolic factors such as pro-inflammatory cytokines, proteolytic enzymes, and chemokines, as well as downregulation of anabolic factors such as anti-inflammatory cytokines and growth factors [42]. Here, we performed IMC on samples from DMM mice treated with LIPO, ORTHO, or PBS (referred to as "UNTREATED" control) to
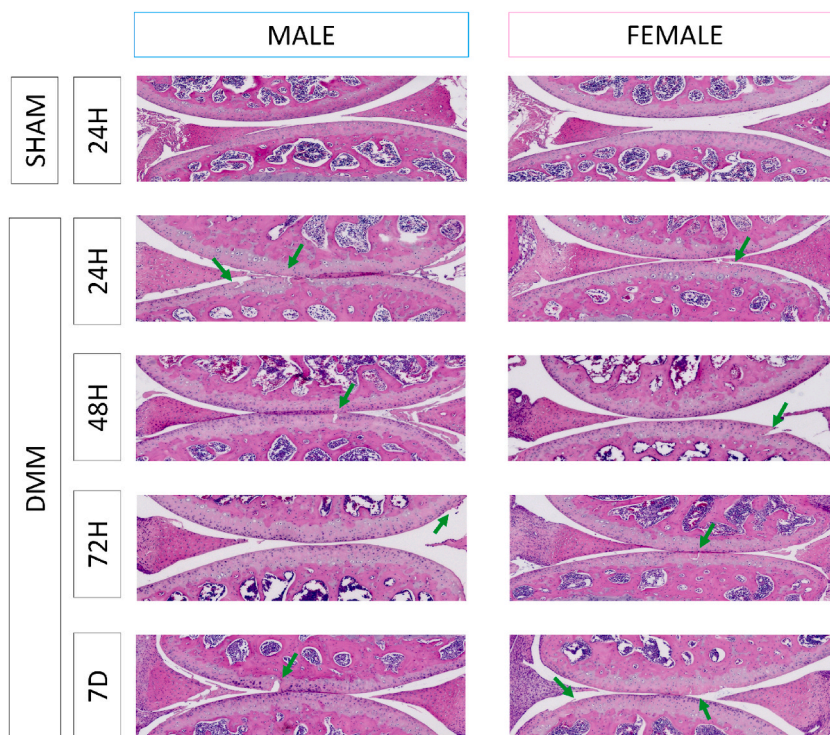
Fig. 6. H&E staining of articular cartilage. Histological sections of legs stained with H&E validated the presence of articular cartilage damage following injury. Left panel represents MALE specimens, while right panel represents FEMALE specimens, while groups and timepoints are reported in the tags. As indicated by green arrows, only the DMM group showed some extent of cartilage damage, while the SHAM group's articular cartilage was healthy. (For interpretation of the references to color in this figure legend, the reader is referred to the Web version of this article.)

dissect the impact of NP administration on tissue inflammation.

IMC is a powerful technique for obtaining comprehensive snapshots of the tissue microenvironment at the single-cell level [43]. Metal-tagged antibodies can be used to stain up to 40 markers on the same tissue slide due to the lack of spectral overlapping typical of traditional fluorescence imaging. We stained for lineage markers related to the immune system environment (CD4, F4/80, and Ly6G) as well as for a pro-fibrotic marker (α-SMA). According to the marker's expression or its absence ("undetermined" event), classification was performed at the pixel level and allowed segmentation of the images. Pooled events from each sample type were then processed with t-distributed stochastic neighbor embedding (t-SNE) statistical analysis to visualize a complex dataset in a two-dimensional (2-D) space. When projecting the identified super-clusters onto a 2-D t-SNE map (Fig. 7a), two different patterns emerged: first, clusters obtained from events belonging to untreated samples had a completely different spatial organization compared with those from samples treated with LIPO and ORTHO; second, Ly6G- and F4/80-associated clusters were clearly identifiable and spatially isolated in the t-SNE obtained from untreated samples, while they were not identifiable in those from treated samples.

The initial classification displayed in Fig. 7a was further refined using several markers (CD11b, CD11c, CD4, CD8, Ly6G, F4/80, CD206, CD163, CD86, Ki67, PDL1, and α-SMA) that allowed us to identify 19 additional cell clusters associated with different cell subsets, mostly belonging to the immune system. Neighborhood analysis was performed to visualize and quantify the spatial inter-action between different immune cell subsets. The neighboring interaction between each cluster is represented as a heatmap (Fig. 7b). Overall, the interactions between clusters were lower in NP-treated samples compared with the untreated samples. In particular, we observed almost no interaction between granulocytes (identified as Ly6G$^+$ and Ly6G$^+$/CD11c$^+$) or dendritic cells (CD11b$^+$/CD11c$^+$, DCs) and the lymphoid cells subsets (identified as either CD4$^+$ T helper cells or CD8$^+$ cytotoxic T cells) or the macrophagic compartment (F4/80$^+$ cells) in LIPO and ORTHO conditions, when compared with untreated samples. In LIPO samples, cytotoxic T cells (CD8$^+$) and T helper cell subsets (CD4$^+$, expressing FoxP3, Gata3, Ki67, or PD1) showed increased interactions, whereas macrophage lineages (F4/80$^+$ cells) clustered together in ORTHO samples.

In the context of OA, the innate immune system is activated when pattern recognition receptors encounter damage-associated molecular patterns generated by the breakdown of cartilage components triggered by trauma [39]. Production of damage-associated molecular patterns can increase when other cell types, including macrophages and chondrocytes, release catabolic factors that cause further tissue damage [40]. The decreased interaction between cells from the myeloid and lymphoid compartment shown in NP-treated samples could be associated with either lower abundance of such damage-associated factors or lower counts of cell types responsible for triggering constant tissue damage, like macrophages. In fact, analyzing cell counts belonging to each cell subset, we observed that NP treatment induced a sharp reduction of the myeloid compartment (CD11b$^+$ cells) compared with the
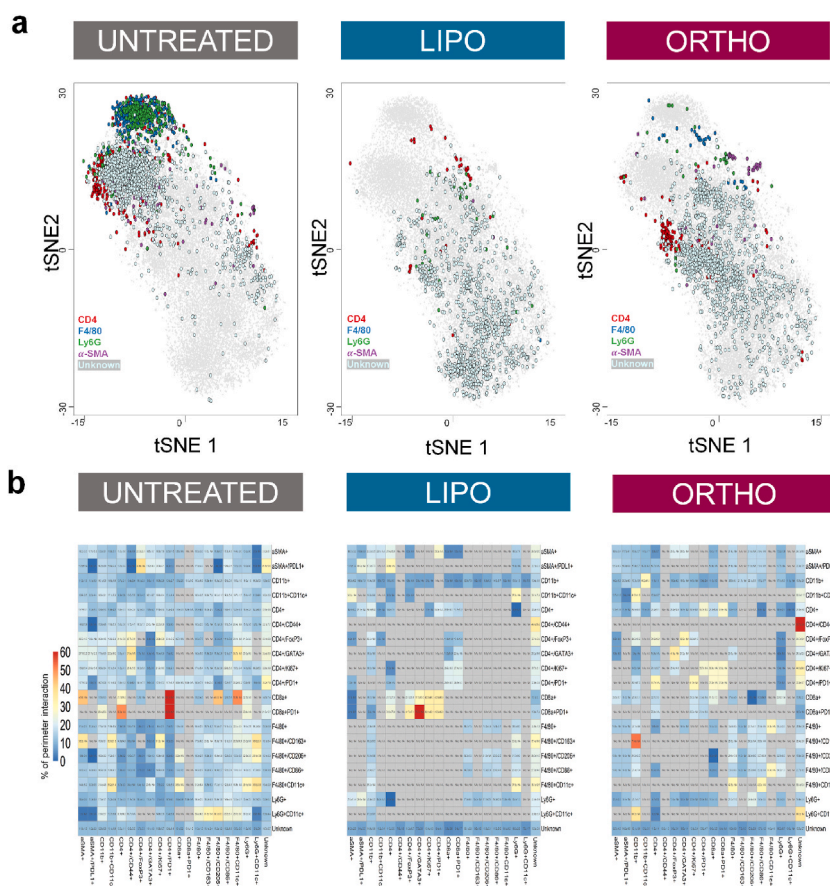
Fig. 7. Imaging mass spectrometry, analysis of immune environment (a) Cells from all the study samples (untreated, LIPO, and ORTHO) were clustered based on their markers' expression levels using a t-SNE algorithm (shaded circles): group-specific cells, colored according to the cell-cluster classification, were represented on the maps. (b) Heatmaps representing the interaction of each cell sub-population (rows) with neighboring cells (columns). The level of interaction is presented as the mean ± SD percent of the perimeter of a cell type touching another cell type.

untreated group (Fig. 8a), and these results were confirmed by evaluating the percent of area (Supplementary Fig. S6). A more comprehensive analysis of the different myeloid subsets revealed that both NP treatments (LIPO and ORTHO) were associated with a significant reduction in granulocytes (identified as Ly6G$^+$, Fig. 8b, left panel) and macrophages (CD11b$^+$/F4/80$^+$, Fig. 8b, middle panel). In the context of OA, a decrease in granulocyte infiltration could be associated with a lower degree of acute synovitis, as neutrophils are immediately recruited in the joint space in acute inflammation [6,40]. Interestingly, only the ORTHO treatment induced a reduction in DCs counts (CD11b$^+$/CD11c$^+$, Fig. 8b, right panel), while there were no significant differences between untreated and LIPO-treated samples for the same cell subset. Consistent with the decrease in macrophage counts, levels of the fibroblast marker α-SMA showed a downward trend in NP-treated samples (Fig. 8c): in fact, macrophages are responsible for the recruitment of fibroblasts to the injured area, as part of the acute phase of inflammation that can degenerate in fibrosis [40]. Notably, NP treatment seems to have triggered the expansion of the M2-like anti-inflammatory macrophage subset (expressing CD206, Fig. 8d). Though there was no significant difference, this upward trend suggests that LIPO and ORTHO revert the composition of the tissue infiltrating F4/80$^+$ cells, which could have serious implications for OA progression. Overall, evidence shows that both LIPO and ORTHO were able decrease cellular infiltration of macrophage lineages and trigger an upward trend of polarization toward an anti-inflammatory phenotype. OA has long been associated with a "chronic wound" environment, where macrophages constantly release catabolic factors and pro-inflammatory cytokines that are known to induce production of catabolic factors (metalloproteinases and aggreca-nases) in chondrocytes [6,39,40]. Because chondrocytes are incapable of repopulating the injured site with sufficient pace, the in-flammatory cascade is never resolved. Here, both biomimetic treatments had an extraordinary effect on infiltration of cells from the innate immune system: a decrease in macrophage infiltration and their polarization towards the M2 anti-inflammatory phenotype could be powerful strategies to slow down or modify disease progression.

We also evaluated the impact of NP administration on the lymphoid compartment. While there was no difference in CD8$^+$ cell counts (Fig. 8e), both LIPO and ORTHO induced a significant reduction in the percentage of CD4$^+$ T helper cells subset compared to the untreated group (Fig. 8f, left panel). Interestingly, CD4$^+$ cells from NP-treated tissues showed a downregulation of CD44 expression (marker of T cell activation, Fig. 8f, right panel), suggesting that the NPs impact the activation of T cells. Finally, no difference in the
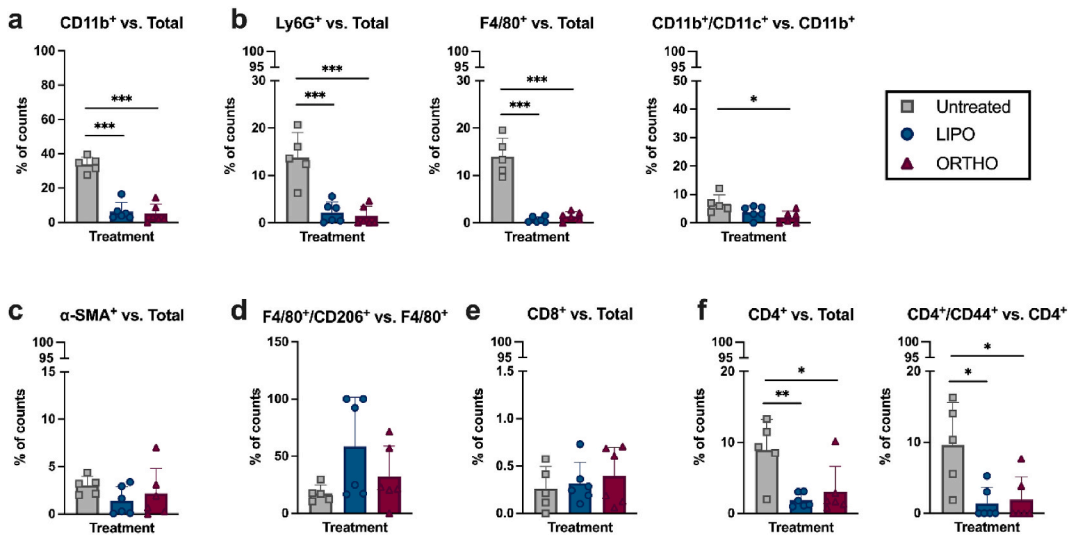
Fig. 8. IMC, NP impact on immune subsets/inflammation (a-f) Graphs representing the percentage of cell counts for the different immune subsets (according to the markers reported in the title of each panel) calculated for untreated, LIPO-treated, and ORTHO-treated samples. Data were analyzed with one-way ANOVA and Tukey post-hoc tests (p-values stylized as: *p < 0.05, **p < 0.01, ***p < 0.001. n = 6, except for untreated samples where n = 5) and are shown as the mean $\pm$ SD.

expression of PD1 (inhibitory receptor), Ki67 (marker of proliferation), FoxP3 (marker of T regulatory cells), or Gata3 (marker of Th2 polarization) was detected amongst different samples (Supplementary Fig. S7). In OA patients, the predominant T cell type is represented by $CD4^+$ T helper cells, while $CD8^+$ cytotoxic T cells counts are lower, giving a higher CD4/CD8 ratio compared with healthy tissues [41]. Although the role of T helper cells in the pathophysiology of OA still needs to be fully elucidated, they have been shown to contribute to the production of catabolic cytokines that participate in the constant cycle of tissue remodeling typical of OA. NP treatment seemed to trigger a downregulation of CD44 expression in T helper cells: a sign that these cells could be exhausted or not functional. Interestingly, CD44 deficiency modulates $CD4^+$ T cell phenotype by inhibiting differentiation towards the pro-inflammatory phenotype (T helper 1, Th1) and promoting differentiation towards the Th2 anti-inflammatory phenotype [44]. In support of the hypothesis that NP treatment induces exhaustion of the $CD4^+$ cell subset, we found that ORTHO treatment reduced the percentage of dendritic cells that are usually involved in the activation of naïve T cells via the major histocompatibility complex I/II. The ability of our treatment to reduce abundance of such cell types within the synovial space could be leveraged into a novel approach to treat OA.

Taken together, these results highlight how both LIPO, and ORTHO, strongly influence the inflammatory environment of the joint when IV administered immediately after injury. Given that the inflammatory environment of the joint has long been recognized as one of the main factors responsible for OA development and progression, having a drug delivery system that can impair inflammation early on, especially without the use of any drug, could put us on the frontline of development of drug delivery systems for OA. It is clear that biomimicry is a key element for developing treatments for OA, and our strategy revealed how just the lipid composition of our drug delivery system LIPO had an extraordinary impact on cellular infiltrates of the injured joint. In fact, LIPO were designed with naturally occurring phospholipids (PC, PG), and the addition of macrophage MPs had very limited additional effects compared with LIPO alone. Different classes of phospholipids have been found in synovial fluid, and they have been shown to contribute to the joint's normal physiology by mediating the "boundary lubrication" phenomenon that decreases friction between joint surfaces, thus preventing cartilage damage [45–48]. After injury, normal phospholipid concentrations of ~0.1–0.2 mg/ml in the synovial fluid fall to ~0.02–0.08 mg/ml: lack of phospholipids could be detrimental for the boundary lubrication process, and replacement therapies could revert this drop in phospholipid concentration. Here, we have shown how IV administration of liposomal formulations displaying naturally occurring phospholipids strongly impacts the tissue inflammatory environment. The building blocks of our biomimetic NPs (phospholipids like DPPC, DSPC, and DOPG) could play an important role in replenishing the phospholipid content within the synovial fluid, thus triggering a positive impact on the development of the pathology down the line. Moreover, the systemic administration can be extended to a multi-trauma condition that is still an open challenge in clinical practice, or translated to related pathologies, such as rheumatoid arthritis.

3. Conclusions

In this work, we pioneered a novel treatment strategy involving IV administration of NPs in the acute phase of PTOA. To the best of our knowledge, this is the first comprehensive study that evaluates the potential of a liposomal-based drug delivery system as a theranostic tool for PTOA via systemic administration. In fact, NPs have superior targeting properties towards injury in a murine model of PTOA. This could be exploited as a diagnostic tool in the clinic, especially in the context of multi-trauma: our biomimetic NPs can

easily be tuned to allow for MRI contrast agents loading, giving immediate readouts on the injury sites when administered IV. In addition, our evidence shows that both LIPO and ORTHO significantly impacted tissue inflammation despite the absence of any therapeutic agent. In the context of OA, where inflammation is one of the key components involved in the development and worsening of the pathology, modulating the inflammatory environment could be a powerful strategy to slow down disease progression or revert its progression upon loading of a drug.

4. Experimental section

4.1. Reagents and materials

DPPC, DSPC, Cholesterol, and DOPG (Avanti Polar Lipids). Chloroform, 2-mercaptoethanol, and $10\times$ PBS (Sigma-Aldrich). 0.22 µm sterile PVDF syringe filters, Rapid Gold BCA protein assay kit, bovine serum albumin, and 29G insulin syringes (Fisher Scientific). Millipore Membrane Protein extraction kit (Milllipore, Sigma). Disposable polystyrene cuvettes, and zeta potential capillary tube cuvette (Malvern, Instruments, Worcestershire, UK). 4–20% Mini-PROTEAN TGX Precast Protein Gels, *Trans*-Blot Turbo Mini Nitrocellulose, $2\times$ Laemmli Sample Buffer, and Clarity Western ECL Substrate (Bio-Rad Laboratories, California, USA).

4.2. Cell culture

J774 murine macrophages (ATCC) were cultured in complete medium (DMEM high glucose with 10% of fetal bovine serum and 1% of penicillin/streptomycin) in humidified incubators (5% CO_2, 37 °C) until a confluency of 70–80%. Cells were detached by scraping and processed for MP extraction.

4.3. MP extraction and quantification

MPs were extracted using the Millipore Membrane Protein extraction kit following manufacturer's instructions. MPs were characterized using the Rapid Gold BCA protein quantification kit: samples loaded in triplicate were compared to a bovine serum albumin standard curve ranging from 0 to 1.5 mg/ml and a plate reader (Tecan) was used to measure absorbance (480 nm).

4.4. NP synthesis

LIPO and ORTHO were synthesized via Thin Layer Evaporation and subsequently extruded to obtain homogeneous size distribution. DPPC, Cholesterol, DSPC, and DOPG were weighed and dissolved in 900 µl of chloroform (molar ratio 49 : 10 : 11 : 30, to a final lipid concentration of 20 mg/ml). NP fluorescence was ensured by adding 100 µl of either Cy5.5-conjugated lipid (for IVM) or Cy7-conjugated lipid (for IVIS) and resuspending in chloroform to a final concentration of 1 mg/ml. To ensure complete dissolution of lipids in chloroform, the solution was sonicated for 3–5 min in a heated bath (45 °C). The solution was then transferred to a 50-ml round bottom flask, and chloroform was completely evaporated using a rotary evaporator (0 psi, 220 rpm, 45 °C) for 30 min. The thin layer was then hydrated using the same rotary evaporator (250 rpm, 45 °C) using $1\times$ PBS for LIPO or a solution of MPs in $1\times$ PBS for ORTHO (frozen MPs were thawed on ice and a volume corresponding to a mass one-fortieth of the one of the lipids was collected and topped up to 1 ml using $1\times$ PBS: this solution was used for the hydration step). Subsequently, both LIPO and ORTHO were extruded using consecutive cycles of polycarbonate membranes (2×400 nm, 3×200 nm, 2×100 nm, and 3×80 nm), maintaining a temperature of 45 °C. Synthesis was followed by dialysis in $1\times$ PBS (4 °C, stirring at 95 rpm) using 1000 kDa float-A-lyzers to remove free-floating lipids and excess of MPs. 1 l of $1\times$ PBS was used for each ml of NPs, and dialysis buffer was changed once after 2 h, and then left overnight. Once retrieved from dialysis, NPs were stored at 4 °C and used within a week.

4.5. NP characterization

Size (nm), PDI (a.u.), and zeta potential (mV) were measured via Dynamic Light Scattering using Malvern Zetasizer. Samples for size and PDI measurements were prepared adding 10 µl of NPs and 990 µl $1\times$ PBS to a semi-microvolume disposable cuvette, while samples for zeta potential were prepared adding 10 µl of sample to 90 µl of $1\times$ PBS and 900 µl of double distilled water (ddH$_2$O, salt concentration was lower to avoid damage to the electrodes of the zeta potential cuvette used for the measurement). For both size and zeta potential, 3 measurements of 15 runs each were acquired and averaged to obtain the final value for each formulation.

4.6. SDS-page

To characterize the protein incorporation within NPs, MPs were purified from the lipid portion to ensure a clean run of the gels. NPs were synthesized as described above and MPs were extracted from them using the "Blight and Dyer" protein purification protocol. Briefly, 200 µl of either LIPO or ORTHO were collected and mixed with 800 µl of methanol. Samples were vortexed, 200 µl of chloroform was added, and samples were vortexed again. After adding 600 µl of ddH$_2$O, samples were vortexed and centrifuged at 14,000 g for 1 min (room temperature). After the centrifugation step, phase separation was achieved: a large aqueous layer on top, a circular flake of protein in the interphase, and a smaller chloroform layer at the bottom (containing the lipid portion of NPs). The top aqueous layer was carefully removed, and 800 µl of methanol was added, followed by vortexing and centrifugation at 20,000*g* for 5 min (room

temperature). Dandruff-like MP precipitates formed against the sides of the tubes of the ORTHO samples. Supernatant was discarded, and dried protein precipitates were dissolved in 30 µl of ddH$_2$O and 30 µl of 2× Laemmli sample buffer (already supplemented with 2-mercaptoethanol). A positive control of 20 µg of MPs was prepared in 1× Laemmli sample buffer. Samples were heated at 96 °C for 5 min, then loaded onto 4–20% Mini-PROTEAN TGX Precast Protein Gels and run for 30 min at 90 V and then for 90 min at 100 V. For the SDS-Page, the protein gel was quickly rinsed in ddH$_2$O, incubated in Coomassie blue stain for 2 h, thoroughly washed in ddH$_2$O for 3 h, and imaged using the ChemiDoc XRS+ System (Bio-Rad).

4.7. Cryo-TEM

NPs were imaged at the Baylor College of Medicine Cryo-Electron Microscopy Core Facility (Houston, TX). Quantifoil R2/1, Cu 200 mesh Holey Carbon grids were pretreated with a 45-s air-glow discharge to make the carbon surface hydrophilic. The use of a Vitrobot Mark IV (FEI, Hillsboro, OR) operated at 18 °C and 100% humidity allowed vitrification of NPs to occur. 3 µl of NP sample was loaded into each grid and blotted for 1–3 s before immersion in liquid ethane. Grids were imaged with a JEOL 3200FS microscope (JEOL) using a Gatan K2 Summit 4kx4k direct detector (Gatan, Pleasanton, CA) and a post-column energy filter set to 30 eV. Images were acquired using a 1-s exposure time.

4.8. Mouse model

Among the different kinds of experimental OA models, the surgically induced DMM model is a well-accepted OA model because of its good reproducibility and a relatively slower progression during OA development. 2-month-old male and female C57BL/6J mice (total n = 240) were purchased from Charles River. Following the acclimation period, mice were randomly divided into 3 groups (n = 10/group): DMM, SHAM, and CONTROL. Mice in the DMM group were given a mild analgesic (buprenorphine SR, 1 mg/kg, sub-cutaneously), anesthetized through isoflurane inhalation, and placed on the surgical bed in the supine position. The right hind limb was draped and sterilized, and the knee joint was exposed by making a 1 cm longitudinal medial para-patellar incision on the skin and a 5 mm longitudinal medial para-patellar incision on the synovial capsule. The lateral dislocation of the patella and patellar ligament were performed with forceps, while holding the hind paw gently and making sure to avoid trauma in the paw. Subsequently, the medial meniscus was identified and dissected using micro-scissors. Finally, both the synovial capsule and the skin were sutured with 6-0 absorbable sutures. In the SHAM group, only the skin was opened without disturbing the synovial capsule. Mice in the CONTROL group were left undisturbed. Mice were then injected retro-orbitally with 100 µl of Cy5.5- or Cy7-labeled LIPO (n = 5) or ORTHO (n = 5) 24 h, 48 h, 72 h, or 7 d after surgery. All animal studies were approved by the Institutional Animal Care and Use Committee (IACUC, protocol #IS00005404) at Houston Methodist Research Institute.

4.9. IVIS imaging

NPs were labeled with Cy7 for IVIS imaging and 6 h after injection, mice were euthanized by CO$_2$ inhalation and subsequent cervical dislocation. Organs (heart, lungs, liver, spleen, kidneys, inguinal lymph nodes, and hind legs) were collected, quickly rinsed in 1× PBS, and imaged on the IVIS system to assess NP targeting and biodistribution. IVIS image acquisition parameters were as follows: Em = 745 nm, Ex = 800 nm, Epi-illumination, Bin: (HR)4, FOV:18.4, f2, 0.5 s. Quantification of IVIS images was performed using the Living Image software.

4.10. IVM imaging

Targeting of ORTHO to OA was evaluated with IVM imaging at the IVM Core at Houston Methodist Research Institute. *In vivo* IVM experiments were carried out according to the guidelines of the Animal Welfare Act and the Guide for the Care and Use of Laboratory Animals as detailed in protocols approved by the IACUC. A Nikon A1R upright laser scanning confocal microscope with a long working distance 4× dry plan apochromat objective, resonance scanner, and motorized and heated stage was used for IVM imaging. Mice were anesthetized with isoflurane before IV injection of NPs and euthanized by CO$_2$ inhalation right after imaging. During imaging, both knees were exposed as described in the surgical section, with the synovial capsule facing upwards to image the area of the injury. 100 µl of Cy5.5-labeled NPs and 25 µl of 0.1 mg/ml FITC-dextran were administered to each animal. Dextran was used as tracer to visualize the vessels and injected 10 min before imaging, while NPs were tracked at 15 min, 45 min, and 6 h post retro-orbital injection.

4.11. Histology

Organs and legs extracted from mice that were administered LIPO and ORTHO were harvested for histology. Following IVIS imaging, organs (heart, lungs, liver, spleen, and kidneys) were immediately transferred into 10% buffered formalin and fixed overnight at 4 °C under stirring conditions. Legs were temporarily stored on ice and later cleaned to remove muscle and ligaments. They were then transferred to 4% paraformaldehyde and fixed overnight at 4 °C under stirring conditions. Once fixed, organs and legs were rinsed in ddH$_2$O and stored in 70% ethanol until they were processed (Shandon Exelsion ES Tissue Processor) and embedded in paraffin (Shandon HistoCenter Embedding System). Organs were sectioned at 20 µm thickness and stained with H&E and legs were sectioned at 5 µm thickness and stained with H&E.

4.12. IMC

Sagittal knee sections from PBS-treated (referred to as UNTREATED), LIPO-treated, and ORTHO-treated animals were subjected to IMC. Tissue sections were incubated at 60 °C for 2 h, deparaffinated in xylene, and rehydrated in a graded series of alcohol concentrations (90–50%, 10 min each). Epitope retrieval was performed by incubating the sections on a heated block at 95 °C in Tris-Tween20 buffer (pH = 9) for 20 min. The sections were incubated with 3% bovine serum albumin tris-buffered saline (TBS) for 1 h (room temperature) to block non-specific binding. They were incubated overnight with a specific metal-conjugated antibodies mix (CD11b, CD11c, CD4, CD8, Ly6G, F4/80, CD206, CD163, CD86, Ki67, PDL1, and α-SMA) at 4 °C. Next, sections were washed 4 times with TBS/0.1% Tween-20. Nuclear counterstaining was performed with Cell-ID Intercalator (Fluidigm) for 5 min, followed by two washes with TBS/0.1% Tween-20. The sections were ablated with Hyperion (Fluidigm) for data acquisition. IMC image analysis was carried out as previously described [49]. Briefly, two random forest models for classification (based on cell type) and regression (based on relative position of a pixel within a cell) were generated on a subset of the study images, training the algorithm to detect cells based on the expression of main lineage markers (i.e., lymphoid markers, CD4 and CD8, myeloid markers, Ly6G and F4/80, and the non-immune marker α-SMA) and creating a prediction map for each cluster. Cell segmentation was then obtained as a progressive agglomeration of pixels of the prediction maps. Cell percentages were calculated as percent of counts and percent of area of a cell sub-type with respect to either the total counts/area of the respective image or the parental population.

4.13. Statistical analysis

NP characterization data were analyzed with an unpaired t-student test ($p \leq 0.05$ was the threshold for statistical significance). Data analysis for animal experiments was performed with two-way ANOVA followed by Tukey's multiple comparisons test ($p \leq 0.05$ was the threshold for statistical significance). Results are reported as mean $\pm$ SD.

Author contribution statement

Chiara Mancino, Francesca Taraballi: Conceived and designed the experiments; Performed the experiments; Analyzed and interpreted the data; Contributed reagents, materials, analysis tools or data; Wrote the paper. Patrick McCulloch, Marco Rasponi, Enrica De Rosa, Anna Pasto, Luigi Dolcetti: Performed the experiments; Wrote the paper; Analyzed and interpreted data; Contributed reagents, materials, analysis tools or data; Wrote the paper.

Data availability statement

Data will be made available on request.

Declaration of competing interest

The authors declare no conflict of interest.

Appendix A. Supplementary data

Supplementary data to this article can be found online at https://doi.org/10.1016/j.heliyon.2023.e16640.

References

[1] A.C. Thomas, T. Hubbard-Turner, E.A. Wikstrom, R.M. Palmieri-Smith, Epidemiology of posttraumatic osteoarthritis, J. Athl. Train. 52 (2017) 491–496.
[2] G.E. Narez, K.M. Fischenich, T.L.H. Donahue, Experimental animal models of post-traumatic osteoarthritis of the knee, Orthop. Rev. 12 (2020).
[3] C.M. Khella, R. Asgarian, J.M. Horvath, B. Rolauffs, M.L. Hart, An evidence-based systematic review of human knee post-traumatic osteoarthritis (PTOA): timeline of clinical presentation and disease markers, comparison of knee joint PTOA models and early disease implications, Int. J. Mol. Sci. 22 (2021) 1996.
[4] L. Haywood, et al., Inflammation and angiogenesis in osteoarthritis, Arthritis Rheum. 48 (2003) 2173–2177.
[5] W.C. Kramer, K.J. Hendricks, J. Wang, Pathogenetic mechanisms of posttraumatic osteoarthritis: opportunities for early intervention, Int. J. Clin. Exp. Med. 4 (2011) 285.
[6] J. Lieberthal, N. Sambamurthy, C.R. Scanzello, Inflammation in joint injury and post-traumatic osteoarthritis, Osteoarthritis Cartilage 23 (2015) 1825–1834.
[7] B. Kurz, et al., Pathomechanisms of cartilage destruction by mechanical injury, Ann. Anat. 187 (2005) 473–485.
[8] L. Punzi, et al., Post-traumatic arthritis: overview on pathogenic mechanisms and role of inflammation, RMD Open 2 (2016), e000279.

[9] C. Auría-Soro, et al., Interactions of nanoparticles and biosystems: microenvironment of nanoparticles and biomolecules in nanomedicine, Nanomaterials 9 (2019) 1365.

[10] L.-P. Wu, D. Wang, Z. Li, Grand challenges in nanomedicine, Mater. Sci. Eng. C 106 (2020), 110302.

[11] S. Su, P.M. Kang, Systemic review of biodegradable nanomaterials in nanomedicine, Nanomaterials 10 (2020) 656.

[12] E. Beltrán-Gracia, A. López-Camacho, I. Higuera-Ciapara, J.B. Velázquez-Fernández, A.A. Vallejo-Cardona, Nanomedicine review: clinical developments in liposomal applications, Cancer Nanotechnol. 10 (2019) 1–40.

[13] Z. Zhao, J.-x. Ma, X.-l. Ma, Different intra-articular injections as therapy for hip osteoarthritis: a systematic review and network meta-analysis, Arthrosc. J. Arthrosc. Relat. Surg. 36 (2020) 1452–1464. e1452.

[14] M.J. Ho, et al., Design and in vivo pharmacokinetic evaluation of triamcinolone acetonide microcrystals-loaded PLGA microsphere for increased drug retention in knees after intra-articular injection, Pharmaceutics 11 (2019) 419.

[15] M.J. Ho, S.R. Kim, Y.W. Choi, M.J. Kang, Recent advances in intra-articular drug delivery systems to extend drug retention in joint, J. Pharm. Invest. 49 (2019) 9–15.

[16] A. Zinger, et al., Enhancing inflammation targeting using tunable leukocyte-based biomimetic nanoparticles, ACS Nano 15 (2021) 6326–6339.

[17] A. Zinger, et al., Bioinspired extracellular vesicles: lessons learned from nature for biomedicine and bioengineering, Nanomaterials 10 (2020) 2172.

[18] P. Van Hoogevest, A. Wendel, The use of natural and synthetic phospholipids as pharmaceutical excipients, Eur. J. Lipid Sci. Technol. 116 (2014) 1088–1107.

[19] N. Krishnan, R.H. Fang, L. Zhang, Engineering of stimuli-responsive self-assembled biomimetic nanoparticles, Adv. Drug Deliv. Rev. 179 (2021), 114006.

[20] C. Corbo, et al., Unveiling the in vivo protein corona of circulating leukocyte-like carriers, ACS Nano 11 (2017) 3262–3273.

[21] J.O. Martinez, et al., Biomimetic nanoparticles with enhanced affinity towards activated endothelium as versatile tools for theranostic drug delivery, Theranostics 8 (2018) 1131.

[22] R. Molinaro, et al., Biomimetic nanoparticles potentiate the anti-inflammatory properties of dexamethasone and reduce the cytokine storm syndrome: an additional weapon against COVID-19? Nanomaterials 10 (2020) 2301.

[23] A. Zinger, et al., Humanized biomimetic nanovesicles for neuron targeting, Adv. Sci. 8 (2021), 2170125.

[24] F. Giordano, et al., Ponatinib loaded leukocyte-based nanoparticles for osteosarcoma treatment in sarcosphere tumor model, Cancer Res. 81 (2021) 311.

[25] A. Zinger, et al., Biomimetic nanoparticles as a theranostic tool for traumatic brain injury, Adv. Funct. Mater. 31 (2021), 2100722.

[26] R. Molinaro, et al., Biomimetic proteolipid vesicles for targeting inflamed tissues, Nat. Mater. 15 (2016) 1037–1046.

[27] R. Molinaro, et al., Design and development of biomimetic nanovesicles using a microfluidic approach, Adv. Mater. 30 (2018), 1702749.

[28] M.H. Laitner, L.C. Erickson, S.f.W. Osteoarthritis, C.P.W. Group, E. Ortman, Understanding the impact of sex and gender in osteoarthritis: assessing research gaps and unmet needs, J. Wom. Health 30 (2021) 634–641.

[29] R.J. Hunter, Zeta Potential in Colloid Science: Principles and Applications, vol. 2, Academic press, 2013.

[30] R. Molinaro, et al., Macrophage-derived nanovesicles exert intrinsic anti-inflammatory properties and prolong survival in sepsis through a direct interaction with macrophages, Nanoscale 11 (2019) 13576–13586.

[31] D.T. Holyoak, Y.F. Tian, M.C. van der Meulen, A. Singh, Osteoarthritis: pathology, mouse models, and nanoparticle injectable systems for targeted treatment, Ann. Biomed. Eng. 44 (2016) 2062–2075.

[32] J.J. McDougall, G. Yeung, C.A. Leonard, C. Sutherland, R.C. Bray, Adaptation of post-traumatic angiogenesis in the rabbit knee by apposition of torn ligament ends, J. Orthop. Res. 18 (2000) 663–670.

[33] D.A. Walsh, C.I. Pearson, Angiogenesis in the pathogenesis of inflammatory joint and lung diseases, Arthritis Res. Ther. 3 (2001) 1–7.

[34] Q. Pan, et al., Characterization of osteoarthritic human knees indicates potential sex differences, Biol. Sex Differ. 7 (2016) 1–15.

[35] C.L. Blaker, E.C. Clarke, C.B. Little, Using mouse models to investigate the pathophysiology, treatment, and prevention of post-traumatic osteoarthritis, J. Orthop. Res. 35 (2017) 424–439.

[36] A. Zinger, et al., Biomimetic nanoparticles as a theranostic tool for traumatic brain injury, Adv. Funct. Mater. (2021), 2100722.

[37] A. Roy, M.J. Ernsting, E. Undzys, S.-D. Li, A highly tumor-targeted nanoparticle of podophyllotoxin penetrated tumor core and regressed multidrug resistant tumors, Biomaterials 52 (2015) 335–346.

[38] J. Spencer, Osteoarthritis. Joint anatomy, physiology, and pathobiology, Vet. Clin. North Am. Small Anim. Pract. 27 (1997) 699–723.

[39] E.W. Orlowsky, V.B. Kraus, The role of innate immunity in osteoarthritis: when our first line of defense goes on the offensive, J. Rheumatol. 42 (2015) 363–371.

[40] J.E. Woodell-May, S.D. Sommerfeld, Role of inflammation and the immune system in the progression of osteoarthritis, J. Orthop. Res. 38 (2020) 253–257.

[41] Y.-s. Li, W. Luo, S.-a. Zhu, G.-h. Lei, T cells in osteoarthritis: alterations and beyond, Front. Immunol. 8 (2017) 356.

[42] C. Bonnet, D. Walsh, Osteoarthritis, angiogenesis and inflammation, Rheumatology 44 (2005) 7–16.

[43] R. Elaldi, et al., High dimensional imaging mass cytometry panel to visualize the tumor immune microenvironment contexture, Front. Immunol. 12 (2021), 666233.

[44] H. Guan, P.S. Nagarkatti, M. Nagarkatti, Role of CD44 in the differentiation of Th1 and Th2 cells: CD44-deficiency enhances the development of Th2 effectors in response to sheep RBC and chicken ovalbumin, J. Immunol. 183 (2009) 172–180.

[45] M.K. Kosinska, et al., A lipidomic study of phospholipid classes and species in human synovial fluid, Arthritis Rheum. 65 (2013) 2323–2333.

[46] D. Mazzucco, R. Scott, M. Spector, Composition of joint fluid in patients undergoing total knee replacement and revision arthroplasty: correlation with flow properties, Biomaterials 25 (2004) 4433–4445.

[47] T.E. Ludwig, J.R. McAllister, V. Lun, J.P. Wiley, T.A. Schmidt, Diminished cartilage-lubricating ability of human osteoarthritic synovial fluid deficient in proteoglycan 4: restoration through proteoglycan 4 supplementation, Arthritis Rheum. 64 (2012) 3963–3971.

[48] T.A. Schmidt, N.S. Gastelum, Q.T. Nguyen, B.L. Schumacher, R.L. Sah, Boundary lubrication of articular cartilage: role of synovial fluid constituents, Arthritis Rheum. 56 (2007) 882–891.

[49] L. Dolcetti, et al., RUNIMC: An R-based package for imaging mass cytometry data analysis and pipeline validation, bioRxiv (2021).